Studies of Self-Absorption in Gamma-Ray Sources

ROBLEY D. EVANS AND RICHARD O. EVANS

Massachusetts Institute of Technology, Cambridge, Massachusetts

I. INTRODUCTION

THE absorption of radioactive radiations, within the emitting source, has been treated previously in quantitative detail for the case of alpha-rays (E1, E2, F2).* The self-absorption of beta-rays is greatly complicated by scattering and can only be treated approximately. Previous work on the self-absorption of gamma-rays within the emitting source has dealt mainly with the corrections to be applied to measurements of compact sources of pure radium salts in small precious-metal containers (H1, O1, P1, P3), or to measurements of radium-residues using specialized apparatus or sample geometry (H2, S2). The large number of artificially radioactive isotopes which emit gamma-radiation, coupled with the appearance of new types of radium assay problems associated with uranium production, have provided the incentive for the following theoretical and experimental evaluation of self-absorption in gamma-ray sources.

II. THEORY OF SELF-ABSORPTION

1. Effects of Geometry, Atomic Number, and Photon Energy on Gamma-Ray Absorption Coefficients

By "self-absorption" we understand here the attenuation of gamma-radiation through the combined effects, within the emitting source, of photoelectric absorption (τ), electron-pair production (κ), Compton absorption (σ_a), and also by deflection of gamma-ray energy through Compton scattering (σ_s). The total Compton cross section for any atom is, of course, the sum of the Compton absorption and of the Compton scattering cross sections for the atom. If the scattered quanta are prevented from reaching the detecting instrument then the attenuation produced by any particular thickness of absorbing material will be maximal. Under these conditions, known in various fields by such terms as "good geometry" or as a "narrow beam" the effective total absorption coefficient will be denoted μ_0, where:

$$\mu_0=\tau+\kappa+\sigma_a+\sigma_s. \tag{1}$$

In almost all practical cases a significant fraction of the scattered quanta do reach the detecting instrument, and the effective absorption coefficient μ will, in general, be somewhat less than μ_0. Special cases will be discussed below in which the attenuating effect of scattering is negligible:

$$\sigma_s=0; \quad \mu=\tau+\kappa+\sigma_a. \tag{2}$$

Other cases can arise in which all scattered quanta reach the detector, and also produce a greater response per quantum than does the harder primary radiation. Under such circumstances σ_s behaves like a negative quantity, and the effective absorption coefficient μ can be even smaller than $\tau+\kappa+\sigma_a$.

Several types of tertiary electromagnetic radiation are also produced in absorbers. Following a pair-production absorption process, the positron may be annihilated within the absorber, giving two 0.51-Mev photons of tertiary radiation. Tertiary radiation also may include significent contributions of x-radiation from atoms which have absorbed a photon by the photoelectric process, as well as of bremsstrahlung from inelastic collisions of secondary Compton electrons or of pair-production electrons with nuclei in the absorber. The combined effects of all types of tertiary photons is also to reduce the value of the effective absorption coefficient.

Whenever a significant proportion of the scattered primary photons or of the tertiary photons actuate the detector, we have

$$\mu<\mu_0, \tag{3}$$

and such experimental conditions are generally referred to as "poor geometry" or as a "wide

* References are to be found at the end of this article.

beam." The variation of the effective absorption coefficient μ for the gamma-rays of radium and its decay products, in two types of "poor geometry," has been given by L. H. Gray (G1) (source buried in a very large mass of aluminum) and by Braestrup (B3) (source buried in lead cylinders of various thicknesses).

Figures 1–3 give the numerical values of the four linear absorption coefficients, τ, κ, σ_a, and σ_s, for photons of various energies in Pb and Al. Bearing in mind that the atomic cross sections vary linearly with atomic number Z for the Compton effect, with Z^2 for pair production, and approximately with Z^4 for photoelectric absorption, the appropriate linear absorption coefficients for all other elements can be computed easily from these curves. Taking the density, atomic weight, and atomic number of the absorber as ρ, W, and Z, and the corresponding numerical constants for lead as 11.35, 207.2, and 82, we have:

$$\tau = \tau_{\mathrm{Pb}}(\rho/11.35)(207.2/W)(Z/82)^4, \quad (4)$$

$$\kappa = \kappa_{\mathrm{Pb}}(\rho/11.35)(207.2/W)(Z/82)^2, \quad (5)$$

$$\sigma = \sigma_{\mathrm{Pb}}(\rho/11.35)(207.2/W)(Z/82), \quad (6)$$

where τ, κ, σ are the linear absorption coefficients in the absorber for photoelectric absorption, pair production, and for either Compton scattering or Compton absorption, while the corresponding values for lead are denoted τ_{Pb}, κ_{Pb}, σ_{Pb} and are to be read from Fig. 2 or 3.

2. Self-Absorption in a Linear Source

In Fig. 4, consider a total amount A of radioactive material distributed uniformly in a linear source of length $2l$, width w, height h, density ρ, hence total mass $M=2whl\rho$. Assume that w and h are small compared with l, and that at the point P on the extension of the long axis of the source, and at a distance a from its center, there

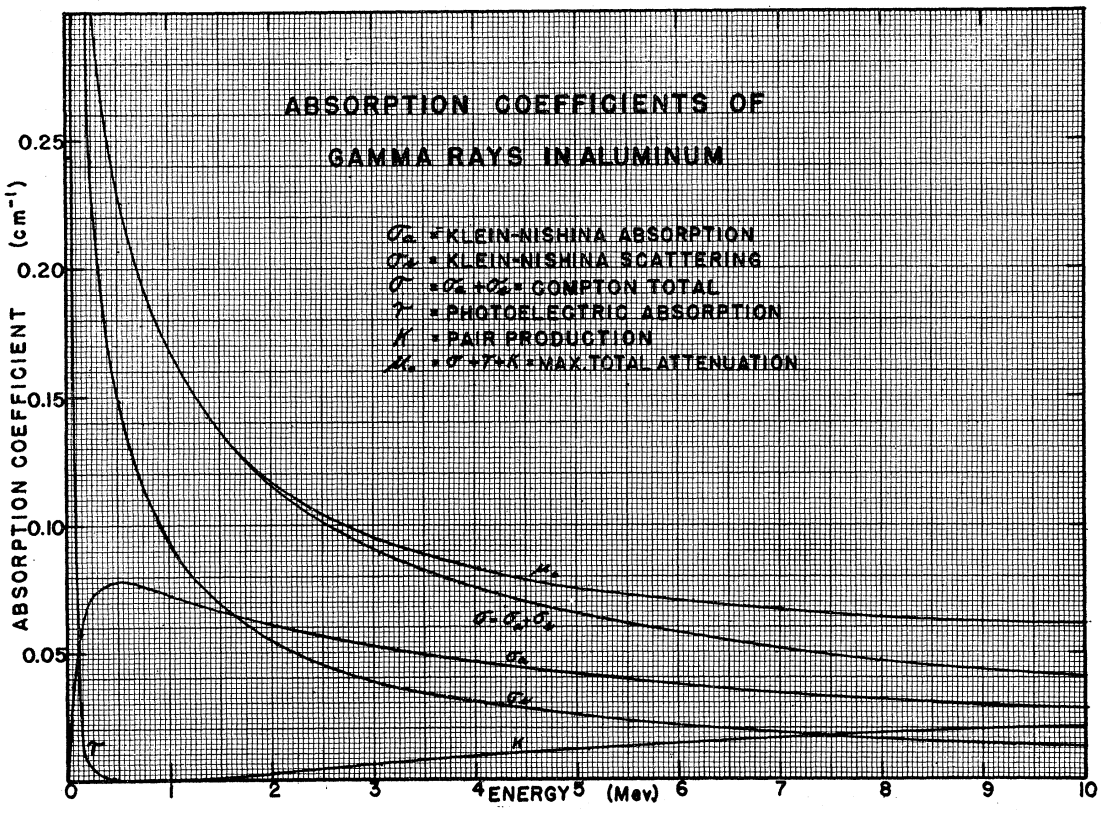

FIG. 1. Linear absorption coefficients for photons of various energies, in Al, taking 7.86×10^{23} electrons per cm^3 Al.

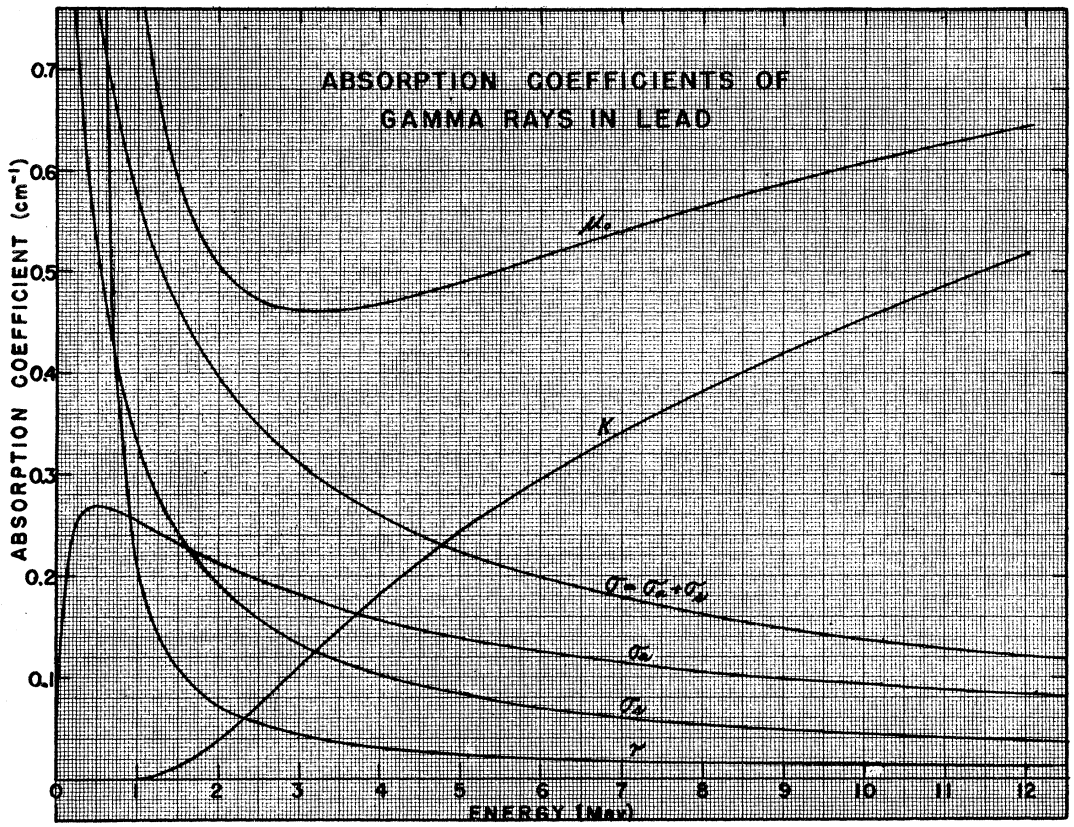

FIG. 2. Linear absorption coefficients for photons of various energies, in Pb.

is a very small gamma-ray counter (or volume element of a larger counter) whose dimensions are small enough to permit regarding the detector as a point. Now if all the radioactive material A were instead concentrated at the distance a from the detector, and if there is no attenuation of the gamma-radiation in the intervening medium, let the counting rate produced be

$$n_0 = kA/a^2, \tag{7}$$

where k is a measure of the sensitivity of the detector. We assume that each element of the extended source is an isotropic emitter of homogenous gamma-rays having only one energy $h\nu$, for which the effective linear attenuation coefficient in the material of the extended source is μ. Finally, we only consider the first collision between emitted primary photons and the electrons and nuclei of the extended source. The attenuation of secondary or scattered photons is ignored for the present. We assume, at first, that the inverse square law holds.

The concentration C of radioactive material per unit volume of source material is then:

$$C = A/2whl. \tag{8}$$

The contribution dn from the element dx at distance $+x$ from the center of the source, to the total counting rate n for the linear source will then be:

$$\begin{aligned} dn &= \frac{kCwhdx}{(a-x)^2} e^{-\mu(l-x)} \\ &= \frac{kA}{a^2} e^{-\mu l}\left[\frac{e^{\mu x}}{(1-x/a)^2}\frac{dx}{2l}\right], \end{aligned} \tag{9}$$

and the total counting rate n for the extended linear source is:

$$n = (n_0 e^{-\mu l}/2l)\int_{-l}^{l} e^{\mu x}(1-x/a)^{-2}dx. \tag{10}$$

When this integrand is expanded, and integrated term by term, we obtain:

$$n=n_0e^{-\mu l}\Big[1\Big(1+\frac{\mu^2l^2}{6}+\frac{\mu^4l^4}{120}+\frac{\mu^6l^6}{5040}+\cdots\Big)+\frac{l}{a}\Big(\frac{2\mu l}{3}+\frac{\mu^3l^3}{15}+\frac{\mu^5l^5}{420}+\cdots\Big)+\frac{l^2}{a^2}\Big(1+\frac{3\mu^2l^2}{10}+\frac{\mu^4l^4}{56}+\cdots\Big)+\frac{l^3}{a^3}\Big(\frac{4\mu l}{5}+\frac{2\mu^3l^3}{21}+\cdots\Big)+\frac{l^4}{a^4}\Big(1+\frac{5}{14}\mu^2l^2+\cdots\Big)+\frac{l^5}{a^5}\Big(\frac{6\mu l}{7}+\cdots\Big)+\frac{l^6}{a^6}(1+\cdots)+\cdots\Big], \quad (11)$$

where n_0 is the counting rate which would be observed if all the radioactive source were at $x=0$, and if self-absorption were zero.

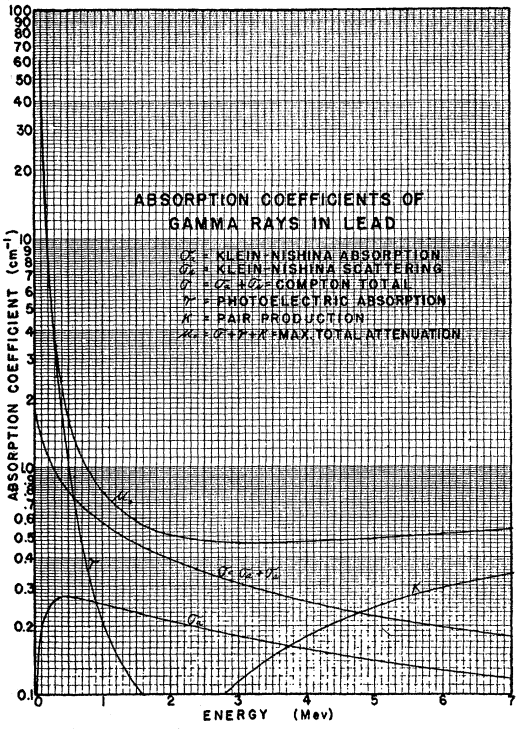

FIG. 3. Linear absorption coefficients for low energy photons, in Pb, taking 27.1×10^{23} electrons per cm³ Pb.

In a number of common practical cases of internal absorption μl may be of the order of 0.1 or less, hence it is of special interest to note that:

$$\text{when } \mu^2l^2\ll1$$

we have, from Eq. (11):

$$n=n_0e^{-\mu l}\Big[\Big(1+\frac{l^2}{a^2}+\frac{l^4}{a^4}+\frac{l^6}{a^6}+\cdots\Big)+\mu l\Big(\frac{2}{3}\frac{l}{a}+\frac{4}{5}\frac{l^3}{a^3}+\frac{6}{7}\frac{l^5}{a^5}+\cdots\Big)+\cdots\Big]$$
$$=n_0e^{-\mu l}\Big[(1-l^2/a^2)^{-1}+\mu l\Big(\frac{2}{3}\frac{l}{a}\Big)\times\Big(1+\frac{12}{10}\frac{l^2}{a^2}+\frac{18}{14}\frac{l^4}{a^4}+\cdots\Big)+\cdots\Big]. \quad (12)$$

The first term in the square bracket of Eq. (12) represents the purely geometrical correction, due to the inverse square law, for the linearly distributed source. For with $\mu=0$, Eq. (12) becomes:

$$n/n_0=1/(1-l^2/a^2)=a^2/(a+l)(a-l), \quad (13)$$

showing that the effective distance between a point detector and an extended uniformly distributed linear source is the geometric mean of the distances from the detector to the near $(a-l)$, and the far $(a+l)$ end of the source. Alternatively, the increase in counting rate due to the geometrical extension of the source is the same as though the source is concentrated at a distance whose squared value is less than a^2, and equal to (a^2-l^2).

The effective attenuation coefficient μ for the thin linear source of Fig. 4 will approach the maximum possible value μ_0 when the width w, and height h are small compared with the length of the source, and when w and h are small compared with the value of $1/\mu'$ appropriate to scattered photons in the material of the source. This is because photons scattered once will, in general, emerge through the sides of the source, at an angle with the axis of the source, and cannot be rescattered by additional source material so as to reach the point detector. Thus the attenuation of the beam of gamma-rays originally directed toward the counter includes the

absorption coefficients τ, κ, σ_a, and the scattering coefficient σ_s.

When the finite size of a cylindrical Geiger-Müller counter is considered, Davis (D1) has shown how the counting rate due to a point source of radioactivity varies with distance. The inverse square law is, of course, valid for distances a between the source and the axis of a counter which are large compared with the half-length b of the counter, when the distance a is normal to the cylindrical axis of the counter. For a/b less than about 3, the inverse square law is to be replaced by an inverse nth power law, where n decreases slowly from 2 to about 1.1 as a/b is decreased to values near 0.3. It is therefore of interest to note that in an extreme case for a linear source near a large counter, and if we assume an inverse first power variation of counting rate with distance, Eq. (10) would be replaced by:

$$n=(n_0e^{-\mu l}/2l)\int_{-l}^{l}e^{\mu x}(1-x/a)^{-1}dx, \quad (14)$$

and that the solution of Eq. (14) which corresponds to Eq. (12) but applies to an inverse first power law, with $\mu^2l^2\ll 1$, is:

$$n=n_0e^{-\mu l}\left[\left(1+\frac{l^2}{3a^2}+\frac{l^4}{5a^4}+\frac{l^6}{7a^6}+\cdots\right)+\mu l\left(\frac{l}{3a}+\frac{l^3}{5a^3}+\frac{l^5}{7a^5}+\cdots\right)+\cdots\right]. \quad (15)$$

In the purely geometrical term we again note the absence of a first-order term in (l/a), and the presence of only even powers of (l/a). Whereas the purely geometrical term for inverse square law varies, by Eq. (12), *exactly* as $(1-l^2/a^2)^{-1}$, the geometrical term for an inverse first power law varies, by Eq. (15), *approximately* as $(1-l^2/a^2)^{-\frac{1}{2}}$.

The effective attenuation coefficient μ, when the detector is of finite size compared with the source-to-counter distance a, may be considerably less than μ_0, because quanta scattered out of the source may still traverse the sensitive volume of the counter. Thus, depending on the relative sizes of the source and of the counter, compared with a, we will find:

$$\mu_0\geqslant\mu\geqslant\mu_0-\sigma_s. \quad (16)$$

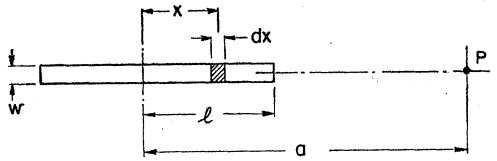

FIG. 4. Schematic representation of a linear source for Eqs. (8) to (16). The source is of height h normal to the plane of the diagram.

3. Self-Absorption in a Cylindrical Source

In the most common practical cases, a radioactive source will have cylindrical geometry, as for example, a liquid or a fine powder in a glass vial. A rigorous and general analytical expression for the self-absorption in a cylindrical source cannot be obtained. The integrals which appear (H1) must be evaluated graphically, or with the aid of tables, for a series of individual numerical values of the attenuation coefficients and dimensions of the source.

It is instructive, however, to develop some approximate analytical solutions. Figure 5 represents a cylindrical source of radius R, and of height h normal to the plane of the diagram, situated with its axis at a distance a from a point detector (or an element of a detector of finite size) at P. We may consider that the source consists of an ensemble of linear sources such as the one shown shaded in the upper sector of the source in Fig. 5. Then the half-length and width of the shaded elements will be:

$$l=R\sin\vartheta, \quad (17)$$

$$w=R\sin\vartheta d\vartheta. \quad (18)$$

To a first approximation, we may consider that the detector element at P responds to gamma-rays originally emitted in a direction parallel to a. This restriction permits us to use the results of Eq. (11) for the radiation from each element. Then the contribution dN, to the counting rate at P, will be:

$$dN_1=kChw2l\Phi e^{-\mu l}/a^2 \quad (19)$$

$$=N_0(2/\pi)\Phi e^{-\mu R\sin\vartheta}\sin^2\vartheta d\vartheta, \quad (20)$$

where Φ represents the square bracket in Eq. (11), and N_0 is the total counting rate to be expected if all the radioactive material were concentrated at the center of the source, and if

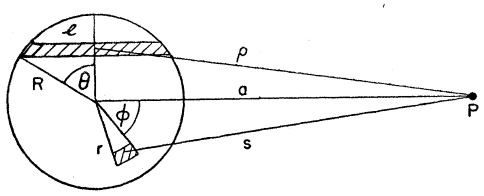

FIG. 5. Schematic representation of a cylindrical source for Eqs. (17) to (31). The source is of height h normal to the plane of the diagram.

there were no self-absorption, that is:

$$N_0 = kC\pi R^2 h/a^2, \tag{21}$$

and all other symbols retain the meaning previously assigned to them. On this model the total counting rate from the cylindrical source will be given by twice the integral of Eq. (20) between the limits of 0 and $\pi/2$ for ϑ. Algebraic expansion of Eq. (20), followed by integration and rearrangement of terms leads to:

$$N_1 = N_0[G_1 - (8/3\pi)\mu R U_1 + (1/2)\mu^2 R^2 V_1 - (32/45\pi)\mu^3 R^3 W_1 + (1/12)\mu^4 R^4 X_1 + \cdots], \tag{22}$$

with:

$$\begin{aligned} G_1 &= 1 + (3/4)R^2/a^2 + (5/8)R^4/a^4 + \cdots, \\ U_1 &= 1 - (3\pi/16)R/a + (4/5)R^2/a^2 \\ &\quad - (3\pi/16)R^3/a^3 + \cdots, \\ V_1 &= 1 - (128/45\pi)R/a + R^2/a^2 - \cdots, \\ W_1 &= 1 - (45\pi/128)R/a + \cdots, \\ X_1 &= 1 - \cdots, \end{aligned} \tag{23}$$

where the purely geometrical correction term G_1 relates only to the approximate inverse square law effects of the finite extension of the source in the plane of Fig. 5. The finite height h of the sample, if comparable with the source-to-detector distance a, would introduce small negative terms, in powers of h/a, into the approximate expression for G_1. Of course, the initial consideration in this model that the gamma-radiation is parallel to a is equivalent to taking geometrical terms in R^2/a^2 as small compared with unity. We shall see from consideration of other models that the numerical coefficients of the power terms in G_1 are a little too large, but are of the correct sign. Note that odd powers of R/a have zero coefficients and are therefore missing.

In Eqs. (22) and (23), U_1, V_1, W_1, X_1 are geometrical correction terms applying to the self-absorption terms which are arranged in powers of μR, and contain both odd and even power terms.

When all geometrical terms are taken as unity, i.e., when $(R/a) \ll 1$, Eq. (22) reduces to the approximate expressions for self-absorption derived by Patterson *et al.* (P1), and by Davis (D1).

A better approximation to the geometrical and self-absorption corrections would be obtained by taking linear elements of the source, as before, but by considering the distance between these elements and the detector as ρ in Fig. 5. Then the contribution dN_2 to the counting rate at P would be:

$$dN_2 = kChw2l\Phi e^{-\mu l}/\rho^2, \tag{24}$$

where:

$$\rho^2 = a^2 + R^2 \cos^2\vartheta. \tag{25}$$

Proceeding as for Eq. (19), we may expand Eq. (24) into a power series in trigonometric functions of ϑ, integrate, and rearrange terms. After a quantity of tedious algebra, there emerges the improved result:

$$N_2 = N_0[G_2 - (8/3\pi)\mu R U_2 + (1/2)\mu^2 R^2 V_2 - \cdots], \tag{26}$$

with:

$$\begin{aligned} G_2 &= 1 + (1/2)R^2/a^2 + (5/8)R^4/a^4 + \cdots, \\ U_2 &= 1 - (3\pi/16)R/a + (3/5)R^2/a^2 \\ &\quad - (5\pi/32)R^3/a^3 + \cdots, \\ V_1 &= 1 - (128/45\pi)R/a + (5/6)R^2/a^2 + \cdots. \end{aligned} \tag{27}$$

Note that the purely geometric term G_2 is of the same form as G_1 of Eq. (23) for the more approximate model which corresponded to the assumption $\rho = a$, but that the numerical coefficient of the correction term in R^2/a^2 is now smaller.

The numerical coefficients of the self-absorption terms in powers of μR in Eq. (26) are unchanged, as are also the numerical coefficients of the first-order geometrical terms R/a in U_2 and V_2. However, these corrections would have been increased if we had been able to give analytical consideration to the slightly longer absorption path traversed by gamma-rays directed along ρ.

As a check on the closeness of the approximation G_2 to the purely geometrical term, we may return to Fig. 5, and employ polar coordinates to integrate the actual effects of elements of area in the plane of the figure. Thus, under the

assumptions that $\mu=0$, and $h \ll a$, the contribution dN_3 to the counting rate at P, from the shaded area element $rdrd\varphi$, is:

$$dN_3 = kChrdrd\varphi/s^2, \tag{28}$$

where:

$$s^2 = a^2[1-(2r/a)\cos\varphi+(r/a)^2]. \tag{29}$$

Expanding Eq. (28) as a power series in $\cos\varphi$ and r, evaluating two times the integral over φ between 0 and π, and over r from 0 to R, we obtain for the purely geometrical term:

$$N_3 = N_0 G_3,$$

with:

$$G_3 = 1+(1/2)R^2/a^2+(1/3)R^4/a^4+\cdots. \tag{30}$$

Thus the second-order geometrical correction term in Eq. (27) is verified as correct. We may regard Eqs. (26) and (27) as a reasonably accurate approximation to the unknown true expression for the geometrical and self-absorption corrections for a cylindrical source. Even so, we have ignored correction terms in h/a relating to the finite height of the source. We have ignored absorption in the walls of any container but will consider these corrections later. We have assumed, by our use of the inverse square law, that the dimensions of the detector are small compared with the source-to-detector distance. In many practical cases a Geiger-Müller counter whose dimensions are comparable with a may have to be used as the detector. Then, as remarked in connection with Eq. (14), Davis (D1) studies of the deviations from the inverse square law for a point source would suggest that solutions to equations similar to Eqs. (24) and (28), but based on an inverse first power law, might be useful for determining lower limits to the geometrical correction terms for a source of finite size near a counter of finite size. This is left as an exercise for the reader.

It may be noted that when a/R is large enough to permit one to ignore the purely geometric terms, and when $\mu R \leqslant 0.12$, as occurs in many practical cases, Eqs. (22) and (26) may be represented within 0.2 percent by the approximation:

$$N = N_0 e^{-(8/3\pi)\mu R}. \tag{31}$$

4. Detection of Scattered Quanta from a Cylindrical Source

We must now consider what numerical values of the gamma-ray linear attenuation coefficient μ are appropriate in the case of a cylindrical source. If the gamma-ray energy is less than 1.6 Mev, Figs. 1, 2, and 3 remind us that the Compton scattering coefficient σ_s will be larger than the Compton absorption coefficient σ_a. If, further, the source material is primarily some substance of small atomic number, such as water or silica, then the photoelectric absorption coefficient, τ, and the pair-production coefficient κ, will both be small compared with σ_a for gamma-ray energies greater than about 0.1 Mev. Thus, in many practical cases the attenuation within the source is principally due to Compton collisions.

If we could use a detector which does not respond to photons having any energy less than that of the primary photons, then every scattered quantum would be ineffective, and $\mu=\mu_0$ as in Eq. (1). Threshold detectors of this type can be used only in a very few special cases. Generally, the scattered photons will actuate the detector, but not with the same efficiency as do the primary photons. Thus the efficiency, ϵ, of the counter for photons of various energies, $h\nu$, becomes important and determines the effective value of μ.

Figure 6 illustrates some typical trajectories for primary photons and scattered or secondary photons. Neglecting the small number of cases

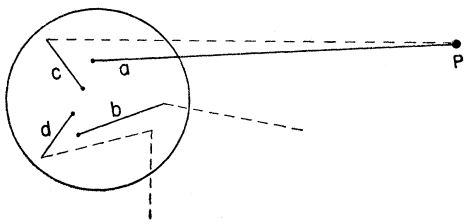

FIG. 6. Schematic representation of Compton scattering within a cylindrical source. Primary quanta are indicated by solid lines, secondary degraded quanta by dotted lines. (*a*) and (*b*) represent primary quanta originally directed toward the counter at P. (*a*) reaches P, but (*b*) is scattered within the source. (*c*) and (*d*) represent primary quanta not originally directed toward the counter but whose secondary quanta do travel toward the counter. The scattered photon from (*c*) reaches the counter, however, the secondary photon from (*d*) is deflected by a second Compton encounter within the source.

in which the primary or secondary photons disappear completely because of photoelectric or pair-production collisions, it is evident that the total number of photons emerging in all directions from the source is the same as the number of primary photons originating in the source. Owing to the circular symmetry of the source, there is no preferred direction in the plane of Fig. 6. Consequently, the number of photons scattered away from the detector is the same as the number scattered toward the director. (If the source were spherical, this generalization would be exact.) Thus, in the energy domain where Compton encounters dominate the attenuation process, the self-absorption within the cylindrical source does not reduce the *number* of quanta reaching the counter.

If the counter were equally sensitive to photons of all energies, i.e., if its efficiency $\epsilon=$const., then there would be no observable self-absorption, and the appropriate value of the apparent linear attenuation coefficient would be $\mu=0$. Actually, no detector is known for which the efficiency is strictly independent of gamma-ray energy. However, a Geiger-Müller counter with a platinum mesh cathode has an efficiency ϵ which decreases very slowly with decreasing photon energy; for a typical (R2) platinum screen-cathode counter, ϵ decreases by only about 40 percent as $h\nu$ decreases from 1.0 to 0.36 Mev. With such a counter, the attenuation coefficient μ would be less than $\sigma_a+\tau+\kappa$.

The sensitivity of a copper-cathode counter is well known to be nearly linear with gamma-ray energy (V1, M3, P2). Then the counting rate of a copper-cathode counter is (nearly) a direct measure of the energy flux of gamma-radiation passing through the counter, and is independent of the number of photons required to produce this energy flux. Now the fractional diminution in the energy flux outside a cylindrical source (e.g., at P in Fig. 6) is simply that fraction of the primary photon energy which is converted into kinetic energy of secondary electrons through Compton absorption, photoelectric absorption, and pair production. The photon energy which is merely scattered will still traverse the counter. Therefore, for a detector having a quantum efficiency proportional to the photon energy, the effective attenuation coefficient within a cylindrical source will be close to:

$$\mu=\sigma_a+\tau+\kappa.$$

If any detector were known whose quantum efficiency ϵ increased with decreasing photon energy $h\nu$, then the scattered quantum from a cylindrical source would be more effective than the more energetic primary quanta and the self-absorption could actually be negative.

In summary: the effective attenuation coefficient μ for self-absorption in a cylindrical source will depend on the quantum efficiency of the detector, and has the following illustrative values if Compton collisions dominate:

$\mu=\mu_0$,	if $\epsilon=0$ for scattered quanta,
$\mu=0$,	if ϵ is constant,
$\mu=\mu_0-\sigma_s$,	if ϵ is proportional to $h\nu$,
$\mu<0$,	if ϵ increases with decreasing $h\nu$.

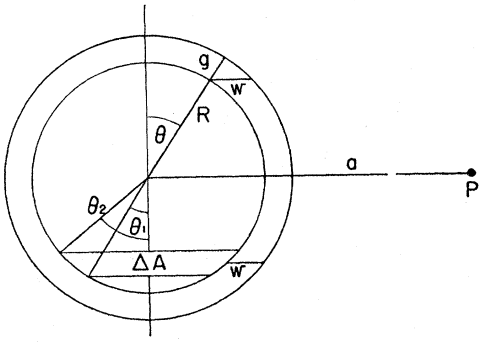

FIG. 7. Cross section of a cylindrical source sourrounded by an absorbing wall of radial thickness g. If the counter is at distance a which is large compared with the radius R of the radioactive source, the path length in the absorbing wall for primary gamma-rays from the volume element ΔA, will be w. See Tables I and II for typical numerical values.

5. Absorption in the Walls of a Cylindrical Source

In many instances the radioactive source will not be a self-supporting cylinder, but will be enclosed in some cylindrical container, as, for example, a radioactive solution in a cylindrical glass vial. Then some additional attenuation of both the primary gamma-rays and of the scattered quanta will occur in the walls. In Fig. 7 we note that most of the primary gamma-radiation passes through the walls obliquely, having a path length w in walls whose radial thickness is only g. Restricting attention to the cases for which the source-to-counter distance,

a, is large compared with the radius, R, of the source, it can be shown easily that:

$$w/g=(R/g)\sin\vartheta \{[1+(g/R)(2+g/R)/\sin^2\vartheta]^{\frac{1}{2}}-1\}. \quad (32)$$

Using Eq. (32), values of the ratio w/g of oblique thickness to radial thickness are given in Table I for several values of the ratio, R/g, of sample radius to radial wall thickness.

Returning to the lower half of Fig. 7, we note that the portion of the radioactive sample which has to send its primary gamma-rays through a particular wall thickness w may be defined in terms of an element of area ΔA, where, from geometry:

$$\frac{2\cdot\Delta A}{\pi R^2}=\frac{2}{\pi}[(\vartheta_2-\vartheta_1)-\tfrac{1}{2}(\sin2\vartheta_2-\sin2\vartheta_1)]. \quad (33)$$

The numerical evaluation of Eq. (33) is given in Table I for 10° intervals from 0° to 90°. We may determine the average effective wall thickness, $\bar{w}$, from

$$\bar{w}=\sum(2\Delta A/\pi R^2)\cdot w, \quad (34)$$

which will be sufficiently accurate in all cases in which the attenuation by the wall is small enough to be essentially linear with wall thickness. Numerical evaluation of Eq. (34) leads to values of $\bar{w}$ which show only a small variation with R/g because the dominant fraction of the sample lies near $\vartheta=90°$; actually, 60 percent of the sample lies between $\vartheta=60°$ and 90° where the effective wall thickness varies only slightly with R/g. The bottom line of Table I gives the average effective wall thickness $\bar{w}$ in terms of the radial thickness g for the range of R/g values met in common glassware. In most practical cases the attenuation $\mu\bar{w}$ in the wall will generally be only a few percent. Consequently, an average value of about $\bar{w}=1.2g$ should suffice in many cases for computation of the attenuation of the primary radiation, provided that $a\gg R$ and that the number of secondary scattered quanta from within the source is small in comparison with the flux of primary quanta. Note that for practical cases $\bar{w}=1.2g$ is a minimum average value. Comparison of Figs. 6 and 7 provides an easy reminder that the average gamma-ray path lengths will be longer than those assumed in Fig. 7 both for primary quanta and for scattered secondary quanta. For experimental arrangements in which the self-absorption is large, so that there are many scattered quanta, and in which the source is close to the counter, the actual effective value of the wall thickness will exceed $1.2g$, and may be estimated as, say, $\bar{w}=1.3g$ to $1.5g$. This should be sufficiently accurate for most cases because the attenuation in the walls can usually be kept down to about 1 to 3 percent, consequently, an uncertainty of 10 percent in the wall thickness correction leads to only about 0.1 to 0.3 percent uncertainty in the measured activity of the sample.

In principle, the wall correction can be determined experimentally by making a series of observations on the same source, but with several wall thicknesses, g, then extrapolating to zero wall. If the sample is in a cylindrical vial or a test tube, then a series of close fitting glass cylinders of various thicknesses can be slid over the vial in order to vary g. In practice, this method is not satisfactory because the effects are so small that sufficiently accurate differential measurements are difficult to obtain. It is usually more satisfactory to calculate the attenuation caused by the wall, using an absorption coefficient appropriate to the primary and secondary photon energies and to the type of detector being used. If these energies are not known, an appropriate absorption coefficient can be measured, using, for example, aluminum absorbers in poor

TABLE I. The ratio w/g of oblique wall thickness to radial thickness, for various values of the ratio of sample radius R to radial wall thickness g. See Fig. 7. The last column gives the fraction of the sample whose path through the wall is w. The bottom line of the table gives the average, or effective oblique wall thickness $\bar{w}/g$ as a function of R/g, as obtained from Eq. (34).

ϑ degrees	w/g $R/g=4$	$R/g=6$	$R/g=8$	$R/g=10$	$2\Delta A/\pi R^2$ for $\vartheta\pm5°$
5	2.67	3.12	3.49	3.79	0.002
15	2.14	2.36	2.55	2.68	0.015
25	1.76	1.88	1.96	2.03	0.040
35	1.48	1.55	1.60	1.62	0.073
45	1.29	1.33	1.35	1.36	0.111
55	1.17	1.19	1.19	1.20	0.149
65	1.09	1.10	1.10	1.10	0.183
75	1.04	1.04	1.04	1.04	0.207
85	1.01	1.01	1.01	1.01	0.220
Weighted average $\bar{w}/g$ from Eq. (34)	1.17	1.19	1.21	1.22	——

geometry (e.g., area several times larger than the source dimensions, $h \times 2R$, placed very close to the source (T1)).

III. MEASUREMENTS OF SELF-ABSORPTION

1. Apparatus

Cylindrical radioactive sources, of 5.5-cm height and with radii varying from 0.39 to 1.25 cm, have been used. Many of the radioactive sources were contained in 12-ml machine-made, soft-glass vials having an inside radius of 0.815 $\pm$0.015 cm and a wall thickness of 0.100$\pm$0.005 cm (supplied by the A. H. Thomas Company, Philadelphia, as 12-ml, 65-$\times$19-mm, No. 9802-G vials). These sources, with their axes vertical,

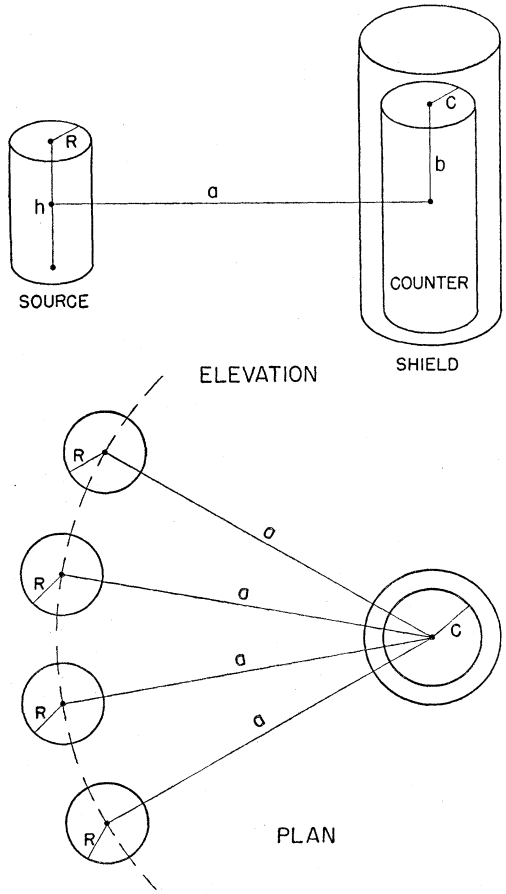

FIG. 8. Schematic arrangement, not to scale, of single counter and multiple sources. For the usual arrangement $a=6$ to 50 cm, $b=6$ cm, $c=1.2$ cm, $h=5.5$ cm, $R=0.39$ to 1.25 cm. The counter shield is a 2.5-inch O.D. aluminum cylinder with 0.25-inch walls, surrounded by various thicknesses of lead.

were supported about 20 cm above the laboratory bench by light balsa-wood stands, and all scattering materials in horizontal directions were minimized.

The detectors have been single Geiger-Müller counters with 60-mesh copper-screen cathodes (E6), usually 12 cm long by 2.0- to 2.5-cm diameter, argon-alcohol filled, and feeding through conventional types of preamplifiers into either self-recording counting-rate meters (K1) or scaling circuits. Thus, the detectors used have had an absolute quantum sensitivity ϵ which is substantially proportional to the photon energy $h\nu$. Absolute calibrations, using Co^{60}, give $\epsilon=0.014$ counts per 1.2-Mev photon traversing the counter normal to its axis. The resolving time of the apparatus was measured by observations on two samples A and B, compared with $(A+B)$ together, for each combination of counter and preamplifier, and was always between 5 and 10 microminutes. All observations were, of course, corrected for counting deficiencies due to the finite resolving time, whenever needed.

The single counter is mounted with its axis vertical and parallel to the axes of the radioactive sources. Especially for weak sources, a number of duplicate sources are used, each being mounted with its axis at the same distance a from the axis of the counter. It has been shown that when two N.B.S. radium standard ampoules are mounted side by side, with their cylindrical walls touching, the additional counting rate due to mutual scattering amounts to 1.5 percent of the total counting rate due to the two ampoules. Therefore, when multiple sources are used, the separation between the axes of adjacent sources is always 4 to 6 times the source radii, in order to effectively eliminate scattering. Our standard arrangement of multiple sources and single counter is shown in Fig. 8. The counter is shielded from beta-rays by an aluminum cylinder, 2.5 inches outside diameter and 0.25 inches wall thickness. Various thicknesses of close-fitting cylindrical lead shielding are added over this permanent aluminum housing for absorption studies.

We have preferred the arrangement of multiple sources and a single counter to the alternative of multiple counters and a single source (D1) because of the well-known additional experimental

complications introduced by parallel operation of a group of counters.

As standards, we have made use of the excellent series of radium standards (C3) distributed by the National Bureau of Standards. These are 5-ml solutions containing various microgram amounts of radium, sealed in Pyrex ampoules having an inside diameter of 11 mm, a wall thickness of 1.5 mm, and a solution height of 5.2 cm.

2. Failure of Inverse Square Law

As would be expected, from Davis (D1) work with point sources and from Eqs. (23), (27), and (30) for finite sources, the inverse square law breaks down when a becomes approximately equal to b. With the apparatus dimensions given in Fig. 8, we find that the apparent activity of the N.B.S. radium standard ampoules is 34 percent less at $a=6$ cm, $(a/b=1.0)$, and 8 percent less at $a=12.7$ cm, $(a/b=2.1)$ than would be expected from the inverse square law applied to measurements at $a=30$ cm, $(a/b=5)$. These variations with source-to-counter distance depend both on geometry and on the degree of self-absorption within the source. A standard 12-ml vial containing 14.7 g of a radium-bearing silicate residue, and therefore having a greater self-absorption than the radium standard, has a measurably smaller variation from the inverse square law (30 percent instead of 34 percent), as is shown in Fig. 9.

This effect is of importance when radium assays are to be made by the gamma-ray method. The ratio of the counting rate for the sample to the counting rate for the radium standard may vary at different source-to-counter distances by several percent, if the sample and the standard vary from one another in size or composition.

3. Attenuation of Gamma-Rays by Lead Absorbers Surrounding the Counter

We have seen from Figs. 6 and 7 and the related discussion that because of symmetry the effective value of the Compton scattering coefficient σ_s will be approximately zero in the source and for cylindrical absorbers surrounding the source, when a copper-cathode detector is used. Finite effective values of σ_s would be expected only when the source or wall thickness is large enough to be comparable with $1/\mu'$, the reciprocal of the attenuation coefficient for the secondary radiation.

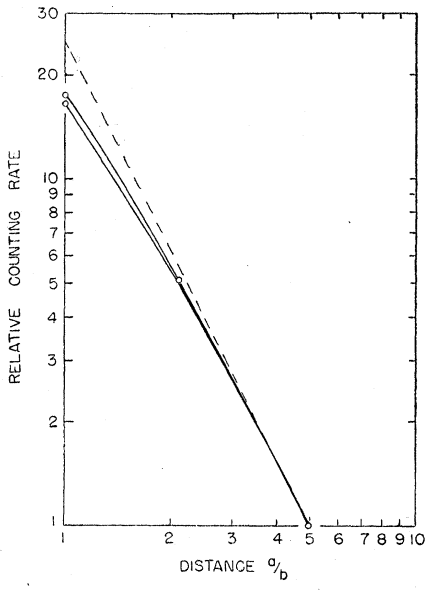

FIG. 9. Empirical variation from inverse square law (upper dashed curve), for the gamma-radiation from a N.B.S. radium standard ampoule (lower curve), and a 12-ml vial containing 14.7 g of a radium-bearing silicate residue (middle curve). The horizontal scale of distance, a, between source and counter is in units of the semilength, b, of the counter. Note that the activity ratio of sample to standard is 4 percent greater at $a=6$ cm $(a/b=1.0)$ than at $a=30$ cm $(a/b=5.0)$. The curves are for zero or for $\frac{3}{16}$-inch lead surrounding the aluminum-counter housing, there being no observable difference between these two conditions.

The effective value of σ_s in an absorber surrounding the detector cannot be predicted as readily. Figure 10 shows the attenuation of the equal mixture of 1.16- and 1.31-Mev gamma-rays of Co^{60} produced by cylindrical lead absorbers surrounding the counter. The observed attenuation coefficient is 0.47 cm^{-1} Pb, for the first $\frac{3}{16}$ inch (4.77 mm), and 0.50 cm^{-1} Pb for the second $\frac{3}{16}$ inch of lead. The theoretical values, for 1.2 Mev photons are: $\kappa=0.00$, $\tau=0.15$, $\sigma_a=0.24$, $\sigma_s=0.28$ cm^{-1} Pb. Thus, within the observational uncertainty, the effective value of σ_s is 0.08 cm^{-1} or $0.3\sigma_s$ for the first $\frac{3}{16}$ inch of lead absorber, and 0.11 cm^{-1} or $0.4\sigma_s$ for the second $\frac{3}{16}$ inch of cylindrical lead absorber surrounding the counter.

Figure 10 also shows the attenuation of the gamma-rays from a typical rich, unaltered

TABLE II. Transmission of gamma-rays emitted by: Co^{60} as an aqueous solution of cobalt chloride; Ra series, as an aqueous solution of radium and its decay products; U series, as a powdered 54 percent uranium ore, bulk density 3.0 g/cc; Th series, as either a powdered thorianite ore containing 33.2 percent thorium and 5.45 percent uranium,* bulk density 3.0 g/cc, or as an old thorium nitrate salt, bulk density 1.6 g/cc; Ac series, as powdered rare-earth salts separated from Colorado carnotite and purified from radium, bulk density 1.8 g/cc. The lead absorbers are cylinders surrounding the 0.25-inch aluminum housing of a copper-screen cathode Geiger-Müller counter (Fig. 8). All measurements made at a source-to-counter distance of $a=30$ cm.

Pb thickness		Gamma-ray transmission				
inches	mm	Co^{60}	Ra^{226} series	U^{238} series	Th^{232} series	Ac^{227} series
0	0	1.000	1.00	1.00	1.00	1.00
1/64	0.04	0.98	0.92	0.94	0.93	0.74
1/32	0.79	0.96	0.84	0.89	0.87	0.54
1/16	1.59	0.93	0.79	0.83	0.82	0.41
1/8	3.18	0.85	0.69	0.73	0.72	0.25
3/16	4.77	0.80	0.62	0.65	0.64	0.18
3/8	9.54	0.63	0.46	0.49	0.47	0.087

* We wish to thank Professor A. M. Gaudin and Dr. D. R. George for the chemical analyses of this ore, and Professor J. W. Irvine, Jr., for the loan of the actinium source.

uranium ore, from actinium and its equilibrium decay products, and from radium and its equilibrium decay products. Except for the radium standard ampoules, each sample was contained in the standard 12-ml vials described earlier.

The gamma-ray transmission data of Fig. 10, together with corresponding values for the thorium series, are given in Table II. It is seen that the attenuation of the gamma-rays from the thorium series is very similar to that of the uranium series. The self-absorption within the uranium ore sample, which is 58 percent uranium and has a bulk density of 3.0 g/cc, is, of course, much greater than in the aqueous radium standard. Consequently the transmission curve in Fig. 10 for the uranium ore lies appreciably above the transmission curve for the radium standard even though their primary photon spectra are substantially identical.

The thorium series data were taken on two types of material, both of which gave substantially identical results. One sample is a thorianite ore, containing 33.2 percent thorium and 5.45 percent uranium, and having a bulk density of 3.0 g/cc. The second sample is thorium nitrate (Eimer and Amend) which was separated more than 30 years ago and in which radioactive equilibrium is therefore nearly re-established. This salt has a bulk density of 1.6 g/cc.

4. Absorption Coefficients for the Gamma-Rays of Radium and Its Decay Products

Radium solutions are widely used as gamma-ray standards. The self-absorption in such stand-

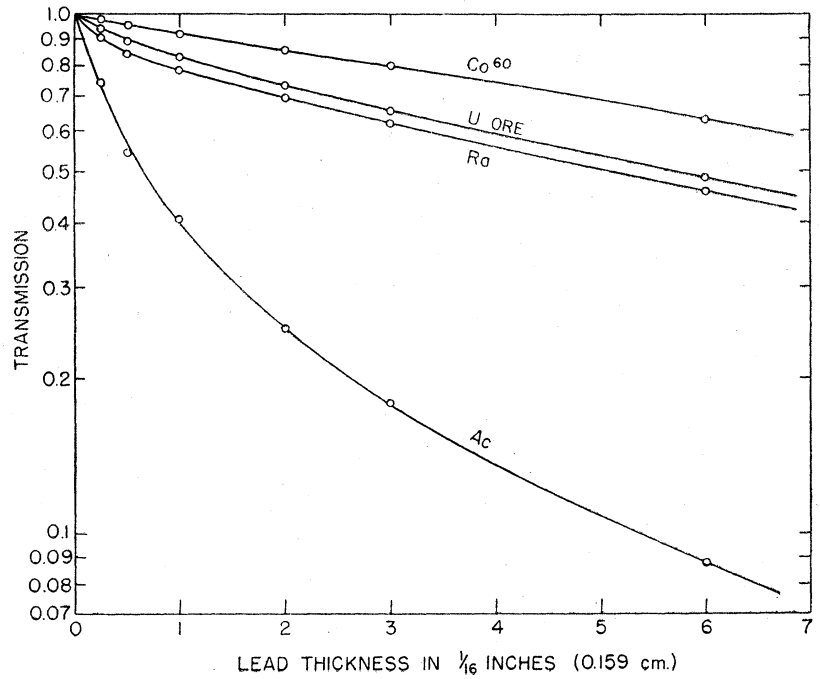

FIG. 10. Transmission of gamma-radiation from Co^{60}, a uranium ore, radium plus its decay products, and actinium plus its decay products, through cylindrical lead absorbers surrounding a copper-cathode Geiger-Müller counter. See Fig. 8 for apparatus arrangement (also Table II).

TABLE III. Observed and computed attenuation coefficients in light elements for the gamma-rays from Ra and its decay products, for various values of Pb filtration surrounding a copper-cathode Geiger-Müller counter.

Attenuation coefficient for γ-rays of Ra and its decay products			Pb filtration surrounding counter: 0	$\frac{3}{16}$ inch (0.477 cm)	$\frac{3}{8}$ inch (0.954 cm)
obs.	μ	cm^{-1} Al	0.089	0.081	0.071
obs.	μ/d	$cm^2\,g^{-1}$ Al	0.033	0.030	0.026
"obs."	μ	cm^{-1} water	0.038	0.035	0.030
theor.	$(\kappa+\tau+\sigma_a)$	cm^{-1} Al	0.071	0.069	0.068
theor.	σ_s	cm^{-1} Al	0.103	0.089	0.082
theor.	μ_0	cm^{-1} Al	0.174	0.158	0.150
theor.	$(\kappa+\tau+\sigma_a+0.2\sigma_s)$	cm^{-1} Al	0.091	0.087	0.084

ards may amount to several percent and will vary with the "filtration" of the gamma-rays in the walls of the detector and in any absorbers used around the detector. For many years it has been customary to use either 5 mm (about $\frac{3}{16}$-inch) or 10 mm (about $\frac{3}{8}$-inch) of lead filtration surrounding the gamma-ray detector when comparing unknown radioactive substances with radium standards.

In agreement with Tarrant's (T1) theory of the relative effectiveness of scattered quanta as a function of absorber geometry, we have found experimentally that the effective absorption coefficient μ for the nearly homogeneous gamma-rays of Co^{60} is

$$\begin{aligned}\mu&=\kappa+\tau+\sigma_a+0.2\sigma_s \\ &=0.00+0.15+0.24+0.06 \\ &=0.45\ cm^{-1}\ Pb,\end{aligned} \tag{35}$$

both when close-fitting cylindrical lead absorbers are placed around the source, and when a large plane layer of absorber is placed directly against the source.

With these geometrical factors established we have measured the attenuation of the radium-series gamma-rays in aluminum absorbers placed at the source, while the counter is shielded by its usual 0.25-inch cylindrical aluminum housing plus various thicknesses of cylindrical lead absorber. Even for the soft components of the RaB-C gamma-rays the photoelectric effect is

TABLE IV. The gamma-ray spectrum(E4) of radium and its decay products. The Compton scattering cross section, $_e\sigma_s$, and the Compton absorption cross section $_e\sigma_a$, are computed from the Klein-Nishina formulas. The total Compton cross section is $_e\sigma=_e\sigma_s+_e\sigma_a$. The photoelectric cross sections, τ, and the pair-production cross sections, κ, for each element have been compiled by C. L. Meaker Davisson (M.I.T., Thesis, 1948) and when combined with the Compton cross sections, lead to the linear and mass absorption coefficients given in the table. Wherever needed, τ and κ can be computed by differences, from the values of $\mu_0=\sigma_s+\sigma_a+\tau+\kappa$ and of σ_s tabulated. The following values for the number of electrons per gram were assumed in computing the table: 2.39×10^{23} for Pb; 2.91×10^{23} for Al; 2.46×10^{23} for Ba; 3.01×10^{23} for SiO_2; and 3.34×10^{23} for H_2O.

Transition			Ra→Rn	RaB→RaC			RaC→RaC′								Total
Energy per photon (Mev)		$h\nu$	0.184	0.241	0.294	0.350	0.607	0.766	0.933	1.120	1.238	1.379	1.761	2.198	
Average quanta per alpha-ray of Ra		n	0.012	0.115	0.258	0.450	0.658	0.065	0.067	0.206	0.063	0.064	0.258	0.074	2.290 quanta
Total photon energy (Mev) per alpha-ray of Ra		$n\cdot h\nu$	0.0022	0.0277	0.0758	0.1575	0.4000	0.0498	0.0625	0.2310	0.0780	0.0882	0.4540	0.1626	1.7893 Mev
Compton cross sections in 10^{-25} cm^2/electron		$_e\sigma_s$	3.31	2.90	2.60	2.35	1.68	1.43	1.24	1.09	1.01	0.92	0.76	0.63	
		$_e\sigma_a$	0.860	0.917	0.947	0.970	0.980	0.962	0.942	0.903	0.886	0.867	0.806	0.755	
Linear absorption coefficients, in cm^{-1}	Al	μ_0	0.337	0.304	0.282	0.264	0.209	0.188	0.171	0.157	0.149	0.141	0.125	0.112	
		σ_s	0.260	0.228	0.204	0.185	0.132	0.112	0.097	0.086	0.079	0.072	0.060	0.050	
	Pb	μ_0	13.4	7.18	4.60	3.22	1.340	1.022	0.837	0.724	0.667	0.615	0.531	0.488	
		σ_s	0.90	0.79	0.70	0.64	0.455	0.388	0.336	0.296	0.274	0.249	0.206	0.171	
Mass-absorption coefficients, in cm^2/g	H_2O	μ_0	0.140	0.128	0.119	0.111	0.0890	0.0800	0.0728	0.0666	0.0635	0.0598	0.0527	0.0470	
		σ_s	0.111	0.097	0.087	0.0785	0.0562	0.0478	0.0414	0.0364	0.0338	0.0308	0.0254	0.0211	
	Al	μ_0	0.125	0.112	0.104	0.0970	0.0774	0.0696	0.0633	0.0581	0.0552	0.0522	0.0463	0.0415	
		σ_s	0.0962	0.0843	0.0755	0.0685	0.0489	0.0415	0.0359	0.0318	0.0292	0.0266	0.0222	0.0185	
	SiO_2	μ_0	0.128	0.116	0.108	0.100	0.0800	0.0720	0.0654	0.0602	0.0572	0.0539	0.0478	0.0427	
		σ_s	0.0996	0.0872	0.0782	0.0707	0.0506	0.0430	0.0373	0.0328	0.0304	0.0277	0.0229	0.0190	
	Ba	μ_0	0.515	0.285	0.195	0.148	0.0807	0.0676	0.0595	0.0536	0.0502	0.0475	0.0423	0.0389	
		σ_s	0.0813	0.0713	0.0639	0.0578	0.0413	0.0352	0.0305	0.0268	0.0248	0.0226	0.0187	0.0155	
	Pb	μ_0	1.18	0.633	0.406	0.284	0.1182	0.0901	0.0738	0.0638	0.0588	0.0542	0.0467	0.0430	
		σ_s	0.079	0.070	0.062	0.055	0.0401	0.0342	0.0296	0.0261	0.0242	0.0220	0.0182	0.0151	
Energy transmitted through lead. $n\cdot h\nu\cdot e^{-\xi y}$ with $\xi=\kappa+\tau+\sigma_a+0.4\sigma_s$. Eq. (40) in Mev per α-ray of Ra.		$y=\frac{3}{16}$-inch (0.477 cm)	——	——	0.0104	0.0408	0.2406	0.0342	0.0462	0.1782	0.0613	0.0706	0.3740	0.1353	1.1918 Mev
		$y=\frac{3}{8}$-inch (0.954 cm)	——	——	0.0014	0.0106	0.1448	0.0235	0.0340	0.1373	0.0482	0.0566	0.3080	0.1128	0.8772 Mev

TABLE V. Self-absorption in the National Bureau of Standards radium gamma-ray standard ampoules when stored and used vertically with a copper-cathode Geiger-Müller counter shielded by 0.25-inch aluminum and by additional lead cylinders of various thicknesses, as in Fig. 8.

Correction terms if 77 percent of the radon is in the liquid	Pb filtration around a copper-cathode counter: none	$\frac{3}{16}$-inch (0.477 cm)	$\frac{3}{8}$-inch (0.954 cm)
liquid: $0.77(8/3\pi)R\mu_{water}$	0.014	0.013	0.011
glass: $0.45(\mu/d)_{glass}$	0.015	0.013	0.012
Total fractional self-absorption	0.029	0.026	0.023

negligible in aluminum, so these results may also be expressed as mass absorption coefficients, and taken as generally representative of the light elements in which Compton collisions are the dominant mode of attenuation. As is well known, hydrogen has an anomalously large mass-absorption coefficient because it has twice as many electrons per gram as have the other light elements. As a consequence water, for example, has 1.15 times as many electrons per gram as has aluminum, and will have 1.15 times as great a mass absorption coefficient. This factor is taken into consideration in the semi-empirical values marked "obs" for the absorption coefficients in water given in Table III, and based on the tabulated values from the measurements made in aluminum.

Table III also presents a group of theoretical results, which compare very favorably with the measured values of the absorption coefficients for aluminum in "poor geometry" and with various values of lead filtration of the radium series gamma-rays.

The theoretical absorption coefficients for aluminum are derived in the following manner. Assume that the absolute quantum efficiency, ϵ, of the detector is proportional to the photon energy $h\nu$, that is $\epsilon = k \cdot h\nu$, and that the detector subtends a solid angle ω measured from a source of gamma-radiation which emits n quanta of energy $h\nu$ per unit time. Let ξ be the effective linear attenuation coefficient of these photons in a lead filter of thickness, y, and let η be their effective linear attenuation coefficient in an aluminum absorber of thickness, z, Then the counting rate, N, due to quanta of primary energy $h\nu$, will be:

$$N = (\omega/4\pi)knh\nu e^{-\xi y}e^{-\eta z}$$
$$= (\omega/4\pi)knh\nu e^{-\xi y}(1-\eta z+\cdots), \quad \text{for } z \ll 1/\eta, \quad (36)$$

and the total counting rate, due to a radioactive source emitting a mixture of gamma-rays containing n_i quanta of energy $h\nu_i$, having attenuation coefficients ξ_i in lead and η_i in aluminum,

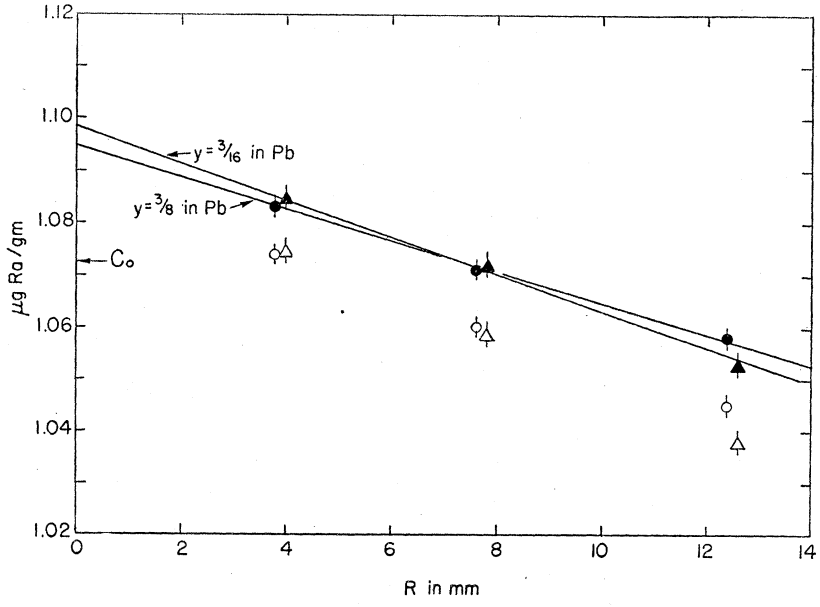

FIG. 11. Individual points (open symbols) for a series of samples of various radii are the measured apparent radium concentrations as compared with the standard radium ampoules. Solid symbols show these points after individual correction for absorption in the glass walls of the various sample containers. Points are shown for two values, $\frac{3}{16}$-inch (triangle) and $\frac{3}{8}$-inch (circles), of Pb filtration. The extrapolated intercepts at $R=0$, diminished by the two appropriate values of the self-absorption in the standard radium ampoule (Table V) give a final corrected value of $C_0 = 1.072\mu g$ Ra/g from each curve.

will be:

$$\sum N=(\omega/4\pi)k[(\sum^{i} n_i h\nu_i e^{-\xi_i y}) - z(\sum^{i} n_i \eta_i h\nu_i e^{-\xi_i y})]. \quad (37)$$

Then the effective linear absorption coefficient, μ, in aluminum is given by:

$$e^{-\mu z}=(1-\mu z+\cdots) = (\sum N)/(\omega/4\pi)k\sum^{i} n_i h\nu_i e^{-\xi_i y}, \quad (38)$$

which reduces to:

$$\mu=(\sum^{i} \eta_i n_i h\nu_i e^{-\xi_i y})/(\sum^{i} n_i h\nu_i e^{-\xi_i y}). \quad (39)$$

We have evaluated Eq. (39) using

$$\xi=(\kappa+\tau+\sigma_a+0.4\sigma_s)_{\mathrm{Pb}}, \quad (40)$$

and for both:

$$\eta=(\kappa+\tau+\sigma_a)_{\mathrm{Al}}, \quad (41)$$

and

$$\eta_0=(\kappa+\tau+\sigma_a+\sigma_s)_{\mathrm{Al}}, \quad (42)$$

to obtain the corresponding values of $\mu=(\kappa+\tau+\sigma_a)$ cm^{-1} Al, $\mu_0=(\kappa+\tau+\sigma_a+\sigma_s)$ cm^{-1} Al, and $\sigma_s=(\mu_0-\mu)$ given in Table III.

The gamma-ray spectrum of radium and its decay products has been compiled previously by one of us (E4) and is given in Table IV together with the attenuation coefficients for each gamma-ray component in several elements, as needed for the evaluation of Eq. (39) and for the theoretical evaluation of self-absorption in radium sources.

It will be noted from Table III that the observed attenuation coefficients for Al absorbers at the source all lie between the two limiting theoretical values corresponding to the inclusion of from zero to one-fifth of the Compton scattering coefficients, σ_s, in Al. The effective attenuation produced by the 0.25-inch Al shield around the counter is probably $\tau+\kappa+\sigma_a+0.3\sigma_s$, because $0.3\sigma_s$ was observed to be the effective fraction of σ_s for cylindrical lead filters surrounding the counter, in the observations on the 1.16- and 1.31-Mev gamma-rays of Co^{60}.

When thick lead filters are used around the counter, a fraction of the Compton-scattered photons produced in the outer layers of the lead will be absorbed photoelectrically without reaching the counter. This effect will be especially pronounced for primary photons of less than about 0.5 Mev, for which the effective Compton scattering coefficient may approach the full value of σ_s. For radium, it will be noted from Table IV that the γ-rays of the RaB→C transition are all softer than 0.5 Mev, and are therefore strongly absorbed in lead. Using for an effective absorption coefficient in Pb surrounding the counter:

$$\mu=(\sum^{i} n_i h\nu_i e^{-\xi_i y})/(\sum^{i} n_i h\nu_i), \quad (43)$$

with ξ as given in Eq. (40), leads to a theoretical transmission $e^{-\mu y}$ for the radium series of 0.67 through $\frac{3}{16}$-inch Pb, and of 0.49 through $\frac{3}{8}$-inch Pb, whereas the observed values (Table II) are 0.62 and 0.46. The ratio of the experimental values for these two thicknesses of lead filter $0.46/0.62=0.74$ and of the theoretical values $0.49/0.67=0.73$ are, however, in good agreement, showing that $0.4\sigma_s$ is a satisfactory choice for the harder components of the gamma-radiation after the soft RaB→C lines have been substantially removed. Even using only $0.4\sigma_s$ in Eq. (40) for ξ, inspection of the separate terms in the summations of Eq. (43) shows that the Ra→Rn and RaB→C gamma-rays account for 15 percent of the total energy of the unfiltered radium-series gamma-rays, while they account for only 4.3 percent of the radiation penetrating $\frac{3}{16}$-inch (0.477 cm)Pb, and only 1.4 percent of the radiation penetrating $\frac{3}{8}$-inch (0.954 cm)Pb. Thus the radium-series gamma-rays which penetrate about 1 cm of Pb consist almost exclusively of the hard gamma-ray lines of the RaC→C′ transition.

5. Self-Absorption in Radium Gamma-Ray Standards

The National Bureau of Standards has issued over a thousand radium gamma-ray standards, containing microgram amounts of radium, as chloride, in 5 ml of water contained in small, flame-sealed glass ampoules. These ampoules vary somewhat in diameter, height of filling, and free gas volume above the liquid. Consequently, their self-absorption, which amounts to about 2 to 3 percent, will vary slightly from lot to lot, and must be evaluated accurately before any particular set of standards can be used for

precision comparison work. The self-absorption will, of course, depend also on the type of detecting instrument used.

The principal gamma-rays arise from decay products of radon, and the radon is distributed partly in the liquid and partly in the free gas volume above the liquid, the proportions depending, in part, on temperature. Therefore care must be taken to store these standards in a vertical position, in order to assure uniform radial distribution of the RaB and RaC during subsequent use.

The self-absorption corrections to be made for any particular ampoule must always include the considerations illustrated below for a representative set of ampoules. When stored and used in a vertical position, at about 70°F, we find by scanning our particular set of standards through a horizontal slit in a 10-cm Pb absorber, that 23 percent of the gamma-rays originate in the free gas volume and 77 percent originate in the liquid. The radius R of the actual liquid filling is computed from the height of filling and knowledge that all the standards are 5 ml, and is 0.55 cm in this set. The outside diameter of these ampoules is 1.40 cm, hence the glass wall thickness, g, is 0.15 cm, and the effective wall thickness, from Table I, is about $\bar{w}=1.2\ g=0.18$ cm, or 0.45 g/cm^2 if the density of the glass is taken as 2.5 g/cm^3. The effective attenuation coefficients are given in the upper half of Table III. Thus the $\frac{3}{16}$-inch (0.477 cm) Pb filtration around a copper-cathode counter, the mass-absorption coefficient applicable to the glass wall is 0.030 cm^2/g, while the mass-absorption coefficient for the water solution is numerically the same as the linear absorption coefficient for water, or 0.035 cm^2/g.

Table V summarizes these various correction terms, and shows a decrease from 2.9 percent self-absorption with no Pb filtration to 2.3 percent self-absorption with about 1 cm of Pb filtration.

6. Dependence of Self-Absorption on Sample Radius

The true values of the corrections for self-absorption can, in principle, always be obtained empirically by obtaining measurements of the apparent activity per gram of material on a series of samples of identical composition but varying radii, and then extrapolating these values to a sample of zero radius. Referring to Eq. (26), we note that if μR and R/a are reasonably small compared with unity, the apparent activity per gram of active material will be a linear function of μR. Figure 11 characterizes the results which may be secured by this method. The radioactive material in this example is a concentrated refinery residue of radium, contained in a finely divided powder which consists mainly of silica and which has a grain density of 2.6 to 2.7 g/cm^3 and a bulk density of 1.09 g/cm^3.

For each value of R, an uncorrected value of the apparent total radium content, and hence radium concentration, is measured. This is then corrected for the glass thickness on the particular sample, making use of Table I and Table III, and is then plotted in Fig. 11. Extrapolation to $R=0$ then gives the radium concentration in the sample in terms of the actual gamma-radiation from the standard radium ampoules. The intercept at $R=0$ must then be corrected for self-absorption in the standard to obtain the true radium concentration in the sample. Two curves are shown in Fig. 11, for $\frac{3}{16}$- and $\frac{3}{8}$-inch Pb filtration. Their intercepts at $R=0$ are not coincident because of the variation of self-absorption in the standard with Pb filtration. Within the experimental error, the intercepts are seen to be in agreement with the decrease of $2.6-2.3=0.3$ percent in self-absorption in the standard, predicted in Table V. The slope of the two curves in Fig. 11, corresponds to the term $(8/3\pi)\mu R$ of Eq. (26) or Eq. (31) and leads to reasonable numerical values of the mass-absorption coefficient, μ/d, which are slightly greater than those of Table IV for SiO_2 because the sample actually contains a few percent of lead salts.

Whenever a series of radium-bearing samples of approximately constant, but unknown, chemical composition and slightly varying bulk density, d, are to be measured for radium content, the method illustrated by Fig. 11 may be used to determine the effective value of the mass-absorption coefficient, μ/d, for the material. Thereafter all similar materials can be packed for measurement in some standard container, such as the 12-ml glass vials described

earlier, and, if the self-absorption corrections are not more than a few percent, the true radium concentration can be computed from a simple linear equation of the form:

$$C_0 = C(1-s)/(1-w-\alpha M) \simeq C(1-s+w+\alpha M), \quad (44)$$

where C_0 and C are the true and the apparent concentrations of radium per gram of sample, s is the fractional self-absorption in the radium standard (Table V), w is the fractional absorption in the glass wall of the sample vial (Tables I and III), M is the mass of the sample contained in the vial, and:

$$\alpha M = (8/3\pi)(\mu/d)(M/\pi Rh). \quad (45)$$

The parameters s, w, and α depend on the gamma-ray detector used as well as on the degree of lead filtration. In case αM is more than a few percent, a second-power term in M will be necessary and can be derived in an obvious way from Eq. (26).

7. Dependence of Self-Absorption on Gamma-Ray Energy

Self-absorption corrections are greatest, of course, for low energy gamma-rays of small penetrating power. Special problems are presented by radioactive substances such as Mn^{52}, Br^{82}, I^{130}, and RaB+C, which emit a number of gamma-ray lines of various energies. Self-absorption corrections can be minimized and, consequently, can be made more accurately, by lead filtration at the detector. Thus soft gamma-ray components can be effectively eliminated by selective attenuation through their preferential photoelectric absorption in lead. The primary gamma-ray spectrum can be distorted into a spectrum consisting essentially of only the harder gamma-ray components, for which the variation of the mass-absorption coefficient with energy and with chemical composition is minimal. The last two lines of Table IV give typical values for the distortion of the RaB+C spectrum, due to lead filtration.

As an extreme example, consider the rich uranium ore of Fig. 10 whose self-absorption of the softer RaB+C gamma-rays is sufficient to give it an apparent over-all transmission curve lying well above the similar curve for the radium standard. In Fig. 10, none of the data are corrected for self-absorption or for glass wall absorption. As the lead filtration is increased, the ratio of the transmission for the U ore to the transmission for the radium standard approaches a constant value of about 1.06, which represents the difference between the self-absorption plus wall absorption principally of the lower energy gamma-rays in the ore sample and in the radium standard. Figure 12 shows these transmission ratios for various lead filter thicknesses, y, plotted against $1/y$ and extrapolated to infinite filter thickness at $1/y=0$.

The physical significance of this ratio becomes clearer if we consider analytically an isotope which emits two gamma-rays, say a high energy gamma-ray having effective linear absorption coefficients of μ_1 in the sample and μ_3 in the standard, and a softer low energy gamma-ray having μ_2 in the sample and μ_4 in the standard. Then if N_0/S_0 is the true ratio of the activity of the sample to that of the standard, while N/S is the observed ratio, and if R and r are the radii of the sample and the standard, then neglecting the wall effect and quadratic terms for simplicity, it can be shown that:

$$N/S = (N_0/S_0)\{1-(8/3\pi)(\mu_1 R-\mu_3 r) -\beta(8/3\pi)[(\mu_2-\mu_1)R-(\mu_4-\mu_3)r]\}, \quad (46)$$

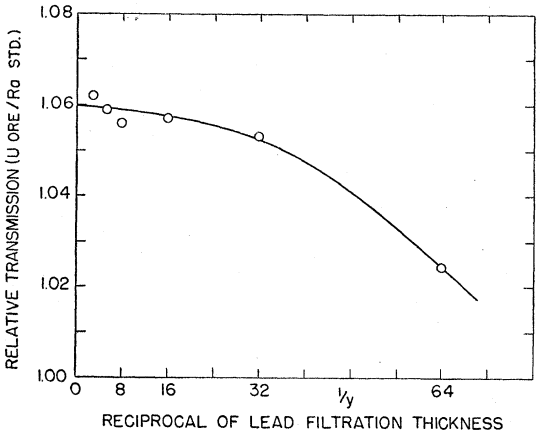

FIG. 12. Transmission through lead filters of thickness y of the gamma-ray from the uranium ore of Fig. 10, relative to the transmission of the gamma-rays from the radium standard. The abscissae is the reciprocal $1/y$ in inches^{-1} of the lead filter thickness. Extrapolation to $1/y=0$ gives the ratio 1.06 corresponding to infinite filtration. The points are based on the original three-figure data rather than on the rounded-off values of Table II.

where β is the fraction of the recorded quanta which are soft quanta. Thus β includes the relative sensitivity of the detector. For a detector whose absolute efficiency is proportional to $h\nu$, β would be the fraction of the total gamma-ray energy reaching the counter which is carried by the low energy quanta. Obviously, β decreases with increasing lead filtration of the mixed gamma-rays. With effectively infinite filtration β becomes zero. Then the transmission ratio N/S depends only on the attenuation coefficients μ_1 and μ_3 of the hard gamma-ray in the sample and in the standard.

The uranium ore of Fig. 12 contains 54 percent uranium, and consequently has a relatively large amount of photoelectric self-absorption of the lower energy gamma-rays. Without detailed knowledge of the chemical composition of the sample, it is difficult to evaluate this large self-absorption very accurately. However, the use of $\frac{3}{8}$-inch lead filtration makes the counter essentially "blind" to low energy radiations. Table IV shows that then 48 percent of the gamma-ray energy reaching the counter is in the 1.761- and 2.198-Mev lines, and over 75 percent is in lines of over 1.1-Mev quantum energy. For these high energies both τ and κ are small compared with σ_a and σ_s, consequently, the mass-absorption coefficients vary only slightly with the chemical nature of the sample, as can be seen from Table IV. A weighted average from Table IV for the effective mass-absorption coefficient in this case is $\mu/d=0.050$ cm^2/g; the sample radius $R=0.815$ cm; bulk density $d=3.0$ g/cm^3; glass-wall thickness $g=0.10$ cm. Consequently, in Eq. (44), $s=0.023$, $w=0.008$, $\alpha M=(8/3\pi)\times(\mu/d)(Rd)=0.104$; the second-order correction term $=(1/2)(\mu/d)^2(Rd)^2=0.007$, and for the observed concentration $C=0.182\mu g$ Ra/g with $\frac{3}{8}$-inch Pb filtration, we have:

$$C_0=0.182(1-0.023)/(1-0.008-0.104+0.007)$$
$$=0.198\mu g \text{ Ra/g}.$$

This is to be compared with the average of seven measurements of this same material by the chemical-solution radon technique (C2) at the National Bureau of Standards and two measurements by the direct-fusion furnace radon technique (E3) at M.I.T.** which gave individual values ranging from 0.189 to 0.203 and averaging $0.199\mu g$ Ra/g. The radon techniques, of course, must operate on very small samples and consequently inhomogeneities in the bulk material may cause a wide variation in the analytical results on a series of individual small samples.

The uranium ore discussed in this section represents an unusually challenging problem in the accurate evaluation of self-absorption, and is taken as confirming the methods developed in the previous sections.

8. Dependence of Self-Absorption on Density and Chemical Character of Sample Material

In a series of samples of finely powdered minerals or of residues from treated uranium ores, the bulk density is usually only about 40 percent of the grain density. It is therefore possible to alter artificially the effective sample density, absorption coefficient, and chemical character of the sample by adding liquids to fill the interstices between the grains. We have used the volatile organic compounds of $_{17}$Cl, $_{35}$Br, and $_{53}$I to obtain significant alterations in the sample density and mean atomic number. The total sample density can usually be raised by about 1 g/cm^3 by the addition of organic liquids, of which the following have been found most suitable, as they are readily removed from samples after use by heating. These addition agents will increase the self-absorption of radium-series gamma-rays in finely powdered samples, packed in the standard 12-ml vials described earlier, by 2 to 7 percent. The effects depend, of course, on the amount of lead filtration used, and are in good quantitative agreement with the principles already described.

		Density g/cm^3	Boiling point °C	Percent halogen by weight
Carbon tetrachloride	CCl_4	1.59	76	92
Ethylene bromide	$C_2H_4Br_2$	2.17	131	85
Ethyl iodide	C_2H_5I	1.93	72	81

** We wish to thank Mr. Robert Giles for carrying out these analyses.

It may be noted that by adding a suitable organic liquid it is possible to alter the density of the sample without appreciably changing the mass-absorption coefficient. Thus, in principle, it is possible to evaluate the self-absorption in the untreated sample, and to determine the true activity of the original sample. However, this procedure rests on small differences between relatively large measured quantities and is not sufficiently accurate to justify routine use as an analytical procedure

9. Estimates of Self-Absorption by the "Two-Vial" Technique

An approximate technique for estimating the self-absorption experimentally is based on the use of 2 standard vials containing the material to be studied. One vial is then used an absorber for the radiation from the other vial. The method is especially useful in those cases in which either the chemical composition of the sample is unknown or where the gamma-ray spectrum of the active isotopes is unknown.

In Fig. 13, let a second cylindrical sample, of identical geometry and having the same chemical composition as the first, be placed in contact with the original sample shown, so that its axis is at a distance $(a-2R)$ from the counter at P. If $a \gg R$ the second sample will almost completely "shadow" the first sample at the counter. Then an integration similar to that of Eq. (19) can be carried out, noting that the radiation from each shaded strip of length $2l$ in the sample at the left of Fig. 13 must pass through a strip of similar length in the second sample. Then the right-hand side of Eq. (19) would be multiplied by $e^{-2\mu_2 l}$, where μ_2 is the attenuation coefficient appropriate to the absorption and scattering in the second sample of radiation originating in the first sample. In general, $\mu_2 > \mu$ because the symmetry of scattered radiation is now lost, and a larger portion of σ_s will be effective in the second vial. When the integration of this modified form of Eq. (19) is carried out, there results for the first-order theory:

$$N = N_0\left(1-\frac{8}{3\pi}\mu R\right)\left(1-\frac{16}{3\pi}\mu_2 R\right). \quad (47)$$

Thus the attenuation produced by the second sample is a little greater than twice the self-absorption in the original sample, because $\mu_2 > \mu$. The second sample also introduces two additional thicknesses of glass wall. Including a small fractional attenuation of w for the glass wall of the first sample, and $2w_2$ for the two glass walls of the second sample, the observed counting rate N_1 in the two-vial geometry of the top diagram in Fig. 14 is:

$$N_1 = N_0\left(1-\frac{8}{3\pi}\mu R - w\right) \times\left(1-\frac{16}{3\pi}\mu_2 R - 2w_2\right)+D, \quad (48)$$

where D is the counting rate due to the radiation originating in the second vial. By swinging the second vial aside, so that it remains at the same distance from P, but does not shadow the first vial, as in the middle diagram in Fig. 14, we evaluate D from the counting rate N_2 for this arrangement:

$$N_2 = N_0[1-(8/3\pi)\mu R - w]+D. \quad (49)$$

Finally, as in the bottom diagram of Fig. 14, the counting rate due to the first vial alone is:

$$N_3 = N_0[1-(8/3\pi)\mu R - w]. \quad (50)$$

Then algebraic combination of these expressions for N_1, N_2, and N_3, gives:

$$(N_2-N_1)/2N_3 = (8/3\pi)\mu_2 R + w_2, \quad (51)$$

which is an overestimate of the correction terms $(8/3\pi)/R+w$ in Eq. (50) because both $\mu_2 > \mu$ and $w_2 > w$. Then the true value of N_0 can be bracketed, as:

$$1 < (N_0/N_3) < 1/[1-(N_2-N_1)/2N_3]. \quad (52)$$

Measurements by this method on both the standard radium ampoules and on ore and radium residue samples, without Pb filtration,

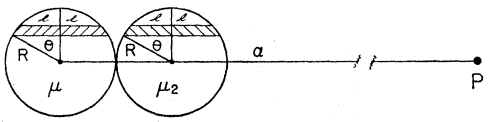

FIG. 13. Schematic representation illustrating the "two-vial" technique for the estimation of self-absorption in one sample (at left) by the gamma-ray attenuation produced in a second identical sample.

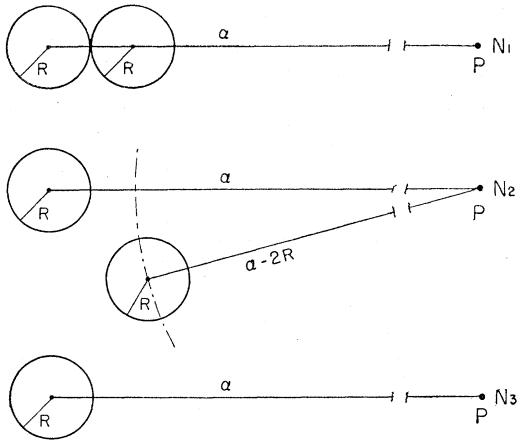

FIG. 14. Schematic arrangement for the measurements to be made using two identical cylindrical samples, for the estimation of self-absorption by the "two-vial" technique. When neither the gamma-ray spectrum nor the chemical composition of the sample is known, this approximate method is particularly useful.

show that the effective value of the attenuation coefficient in the second vial is about:

$$\mu_2=\tau+\kappa+\sigma_a+0.6\sigma_s, \tag{53}$$

whereas in the first vial μ has its usual value of about:

$$\mu=\tau+\kappa+\sigma_a+0.2\sigma_s. \tag{54}$$

IV. RADIUM ASSAY BY GAMMA-RAY MEASUREMENTS

The accurate evaluation of self-absorption in gamma-ray sources facilitates quantitative measurements on many radioactive isotopes. In particular, it makes possible the measurement of radium-bearing materials with sufficient accuracy to compete with and supplement the well established analytical methods for radium based on the measurement of radon (E3, C2).

1. Comparison with Radon Method

In contrast with radon methods, the gamma-ray analyses of radium may be carried out repeatedly on the same sample of material, no chemical treatment or direct-fusion furnace is required, and the sample is not destroyed or modified.

The accuracy of gamma-ray measurements on materials of moderate or low specific activity depends directly on the accuracy with which the corrections for self-absorption can be made. These can usually be obtained now to within a few tenths of one percent, so that the gamma-ray method can have the same accuracy as radon methods.

The sensitivity of radon methods is very high. As little as 10^{-13} curie of radon is readily measurable, and an accuracy of one percent or better can be obtained easily on a total amount of 10^{-12} curie of radon. The gamma-ray method requires much larger total quantities of radium, usually of the order of 10^{-9} g Ra, but the specific activity can be as low as 10^{-11} to 10^{-12} g Ra/g in extreme cases (E6). At these lowest specific activities, the self-absorption corrections may be very large. Internal standardization by the addition of known small amounts of radium may then be necessary.

For materials of high specific activity, very small samples must usually be taken for radium analysis by the radon method. This leads to errors due to variations caused simply by inhomogeneity in the original sample material. The gamma-ray method usually uses between one and a thousand grams of material, and therefore often gives a better average value of the radium content.

2. Effects of Common Radioactive Impurities

There are no known significant gamma-rays associated with the higher members of the U^{238} series above Ra^{226}, except those associated with the β-decay of UX_1, UX_2, and UZ. The gamma-rays of UX_1 are emitted in only about one percent (F1) to 15 percent (B4) of the transitions of UX_1 and are of only about 0.09 Mev. A small additional amount of gamma-radiation is associated with the probable isomeric decay (F1) of 0.15 percent of UX_2 to UZ, which subsequently gives 2 quanta, of about 1 Mev, per disintegration. To verify the expectation that these gamma-rays are negligible in comparison with the gamma-rays of radium and its decay products, we measured the total gamma-radiation from 54 g of uranium as uranyl nitrate (Merk; C.P.) of unknown age since separation. Only a very weak activity was detectable, corresponding to 2 percent of what would be expected if this amount of uranium had been in equilibrium with radium

and its decay products. Even this small activity is probably due almost entirely to radium or other radioactive impurities.

Potassium emits (G2, G3) about 3 quanta of approximately 1.5 Mev gamma radiation per gram per second, due to electron capture in the rare isotope, K^{40}. One gram of ordinary potassium produces in our apparatus the same counting rate as 0.8×10^{-10} g radium with zero lead filtration, or 1.2×10^{-10} g radium with $\frac{3}{8}$-inch lead filtration. Comparison with a known quantity of Co^{60} shows that one gram of potassium gives the same counting rate in our copper-cathode counters, using either 0, $\frac{3}{16}$-, or $\frac{3}{8}$-inch lead filtration, as do 2.00 ± 0.05 disintegrations per second of Co^{60}. If the gamma-ray energies of Co^{60} are (M2) 1.16 and 1.31 Mev, and if the counter sensitivity is linear with photon energy, then these observations show that 1 gram of potassium emits 4.9 ± 0.1 Mev of gamma radiation per second. Thus in most radium assays no correction need be made for potassium.

The actinium series, originating in U^{235}, contains several isotopes which emit gamma-radiation. The fine structure of the α-rays of $_{90}RdAc^{227}$, $_{88}AcX^{223}$, and $_{86}An^{219}$ is, of course, associated with gamma-ray emission, but all of these gamma-rays have quantum energies of less than 0.4 Mev. They are therefore easily eliminated by lead filtration. The gamma-rays associated with the β-ray decay of AcB$\rightarrow$C involve (S1, S3) about 13 quanta of 0.829 Mev, 6 quanta of 0.425 Mev, and 6 quanta of 0.404 Mev per 100 α-rays of An, while the AcC$\rightarrow$C$''$ transition adds only about 15 quanta of 0.35 Mev per 100 α-rays of An. Bearing in mind that there are (N1) only 4.6 disintegrating atoms of An per 100 disintegrating atoms of Ra, the total gamma-ray emission from AcB and AcC amounts to only about 0.010 Mev per disintegrating atom of Ra when the uranium and actinium series are in equilibrium in a primary ore. From the α-ray fine-structure data (C1, L1), it can be computed that when the U^{235} and U^{238} series are in radioactive equilibrium, as in an unaltered uranium ore, the total gamma-ray energy per disintegrating atom of U^{235} or An is 0.160 Mev for RdAc, 0.059 Mev for AcX, and 0.053 Mev for An. When each of these is multiplied by the activity ratio, 0.046, between the actinium and uranium series, and added to the 0.010 Mev due to AcB and AcC, one obtains a total of 0.022 Mev for all the known gamma-rays of the U^{235} or actinium series, per disintegrating atom of U^{238} or of radium. Thus the total energy of the actinium series gamma-rays is only 1.25 percent of the total energy (1.789 Mev) of the radium series gamma-rays, when both series are in equilibrium.

The response of any detector whose quantum efficiency is proportional to $h\nu$, such as a copper-cathode Geiger-Müller counter, is proportional to the total gamma-ray energy traversing the counter. Comparison of these gamma-ray energies and the transmission data of Table II and Fig. 10 shows that for an unaltered uranium ore the contribution of the gamma-rays of the actinium series to the total counting rate of a copper-cathode counter is only 1.25 percent for zero Pb filtration, 0.36 percent for $\frac{3}{16}$-inch Pb filtration, and 0.23 percent for $\frac{3}{8}$-inch Pb filtration, even if the preferentially greater self-absorption of the softer actinium series gamma-rays is neglected.

Returning to Fig. 11, we note that if these samples had contained actinium and its equilibrium decay products, the slopes of both curves would have been slightly steeper, and the intercepts at $R=0$ would have been slightly more widely separated. These effects are greatly accentuated in similar curves for zero Pb filtration, from which the gamma-ray contribution from actinium can be evaluated directly if desired.

As is well known (S3) the thorium series of radioactive elements includes the strong gamma-ray emitters, $MsTh_2$ and Th(B+C$''$) which, respectively, account for about 36 percent and 64 percent of the gamma-ray energy (M1). Table II confirms the observations of many others regarding the close similarity of the transmission curves for the gamma-rays of the thorium and the uranium series. Methods have been developed for distinguishing between thorium and uranium series gamma-rays by the preferential transmission through very thick Pb filters (B2) of the 2.6-Mev gamma-ray of ThC$''$, or by differential ionization chambers having Pb and Al walls (F3). Thus far these methods have only been applicable to strong sources of MsTh or Ra. It does seem possible that a technique

could be developed for weak sources using the differential response of platinum-cathode and of copper-cathode Geiger-Müller counters, which have different spectral sensitivities for gamma-rays, but we have not explored this problem experimentally.

Our measurements on the thorianite ore described in Table II give 0.16 microgram of Ra, or 0.47 gram of uranium plus its decay products as the gamma-ray equivalent of one gram of thorium plus its decay products. This ratio is very close to the value of 0.43 g U/g Th obtained by McCoy and Henderson (M1), using an ionization chamber, and is appreciably smaller than the value of 0.59 g U/g Th found by Evans and Mugele (E6) using copper-cathode Geiger-Müller counters and large cylindrical sources surrounding the counter.

It is a fortunate circumstance that most uranium ores contain substantially no thorium, so that interference by Th is seldom encountered in gamma-ray measurements on uranium ores or products. Conversely, however, all known thorium ores contain an appreciable proportion of uranium, so that gamma-ray techniques are never adequate for the differential assay of thorium alone in a thorium mineral. Here additional techniques (E1, E2, E5, B1), employing alpha-rays, beta-rays, or radon analyses must be employed.

ACKNOWLEDGMENT

We are especially grateful to Mrs. Charlotte Meaker Davisson for checking all the derivations and tables.

BIBLIOGRAPHY

B1. R. F. Beers, Thesis, Massachusetts Institute of Technology (1943).
B2. W. Bothe, Zeits. f. Physik **24**, 10 (1924).
B3. C. B. Braestrup, Radiology **46**, 385 (1946).
B4. H. Bradt and P. Scherrer, Helv. Physica Acta **19**, 307 (1946).
C1. P. Curie and M. S. Rosenblum, Comptes Rendus **196**, 1598 (1933).
C2. L. F. Curtiss and F. J. Davis, J. Research Nat. Bur. Stan. **31**, 181 (1943).
C3. L. F. Curtiss, C. Goodman, A. L. Kovarik, S. C. Lind, C. S. Piggot, R. D. Evans, Phys. Rev. **57**, 457(L) (1940).
D1. F. J. Davis, J. Research Nat. Bur. Stan. **38**, 513 (1947).
E1. R. D. Evans, Phys. Rev. **45**, 29 (1934).
E2. R. D. Evans, Phys. Rev. **45**, 38 (1934).
E3. R. D. Evans, Rev. Sci. Inst. **6**, 99 (1935).
E4. R. D. Evans, Nucleonics **1**, 32 (October 1947).
E5. R. D. Evans, G. D. Finney, A. F. Kip, and R. A. Mugele, Phys. Rev. **47**, 791(A) (1945).
E6. R. D. Evans and R. A. Mugele, Rev. Sci. Inst. **7**, 441 (1936).
F1. N. Feather and E. Bretscher, Proc. Roy. Soc. London **165A**, 530 (1938).
F2. G. D. Finney and R. D. Evans, Phys. Rev. **48**, 503 (1935).
F3. I. Frank, J. Phys. U.S.S.R. **9**, 123 (1945).
G1. L. H. Gray, Proc. Roy. Soc. London **159A**, 263 (1937).
G2. L. H. Gray and G. T. P. Tarrant, Proc. Roy. Soc. London **143A**, 681 (1934).
G3. E. Gleditsch and T. Gráf, Phys. Rev. **72**, 640L (1947).
H1. M. Holuba, Akad. Wiss. Wien., IIa, **146**, 285 (1937).
H2. W. J. Hushley and W. R. Dixon, Can. J. Research **A25**, 210 (1947).
K1. A. F. Kip, A. C. Bousquet, R. D. Evans, and W. N. Tuttle, Rev. Sci. Inst. **17**, 323 (1946).
L1. W. B. Lewis and B. V. Bowden, Proc. Roy. Soc. London **145A**, 235 (1934).
M1. H. N. McCoy and L. M. Henderson, J. Am. Chem. Soc. **40**, 1315 (1918).
M2. L. C. Miller and L. F. Curtiss, J. Research Nat. Bur. Stan. **38**, 359 (1947).
M3. H. Maier-Leibnitz, Z. Naturforsch. **1**, 243 (1946).
N1. A. O. Nier, Phys. Rev. **55**, 150 (1939).
O1. T. H. Oddie, Proc. Phys. Soc. London **51**, 905 (1939).
P1. C. C. Patterson, J. W. T. Walsh, and W. F. Higgins, Proc. Phys. Soc. London **29**, 215 (1917).
P2. W. C. Peacock, Thesis, Massachusetts Institute of Technology (1944).
P3. W. E. Perry, Proc. Phys. Soc. London **57**, 178 (1945).
R1. A. Roberts, J. R. Downing, and M. Deutsch, Phys. Rev. **60**, 544 (1941).
R2. A. Roberts, L. G. Elliott, J. R. Downing, W. C. Peacock, and M. Deutsch, Phys. Rev. **64**, 268 (1943).
S1. B. W. Sargent, Can. J. Research **A17**, 82 (1939).
S2. W. A. Sokolow, Zeits. f. Physik **54**, 385 (1929).
S3. J. Surugue, J. de phys. et rad. **7**, 143 (1946).
T1. G. T. P. Tarrant, Proc. Camb. Phil. Soc. **28**, 475 (1932).
V1. G. F. v. Droste, Zeits. f. Physik **100**, 529 (1936).